mediated by soluble factors may not be involved in synapse destabilization or, alternatively, factors we have not yet tested play a critical role. It is also possible that cytokines or chemokines we tested are indeed involved in synapse remodeling, but the concentration sufficient for exerting their effect is below the limit of detection.

In this study, we found that mild and transient peripheral inflammation induced long-lasting changes of spine dynamics over a period of several weeks and persistent up-regulation of Iba1 expression in microglia. Although we could not demonstrate convincing evidence for the interrelationship between these two alterations, recent findings showing the interaction between microglia and synapses (17-19) indicate that activation of microglia may be associated with spine remodeling. However, the relationship between microglia and spine changes in our present study remains to be fully elucidated in future experiments. The parallel sustained alterations of both spine turnover and the state of microglia in vivo may underlie long-term cognitive impairment after peripheral inflammation, which may be relevant to the neurological problems of patients who have recovered from septic conditions.

Conclusions

In this study, we used *in vivo* two-photon imaging in mice to test whether peripheral immune responses affected cortical synapses. We observed parallel increases in spine dynamics and microglial activities after LPS treatment. Although a more definitive causal relationship between spine and microglial changes should be clarified in the future, our results implicate that microglial activities may affect spine dynamics. These observations could help our understanding of the long-term cognitive impairment of septic human patients.

List of abbreviations used

GFAP: glial fibrillary acidic protein; GFP: green fluorescence protein; Iba: ionized calcium binding adaptor molecule; IL: interleukin; LPS: lipopolysaccharide; LTD: long-term depression; LTP: long-term potentiation; TNF: tumor necrosis factor.

Acknowledgements

We thank Joshua R. Sanes for the *Thy1-GFP* M mouse, together with Ryuichi Shigemoto and Haruo Kasai for transfer of available animals. We thank Wen-Biao Gan and Feng Pan for teaching surgical methods. We thank Aya Ito-Ishida for comments on the manuscript and Ayako Hayashi for help in image analysis. This work was supported by Grants-in-Aid for Scientific Research (18200025, 20019013, 21220008, and 22650070 to S.O.) from the Ministry of Education, Culture, Sports, Science and Technology of Japan and in part by Global COE Program (Integrative Life Science Based on the Study of Biosignaling Mechanisms), MEXT, Japan. A part of this study is the result of "Development of biomarker candidates for social behavior" carried out under the Strategic Research Program for Brain Sciences by the Ministry of Education, Culture, Sports, Science and Technology of Japan (S. O.), and also by Takeda Science Foundation (S. O.).

Author details

[1]Department of Cellular Neurobiology, Graduate School of Medicine, University of Tokyo, Bunkyo-ku, Tokyo 113-0033, Japan. [2]Department of Neurochemistry, National Institute of Neuroscience, Kodaira, Tokyo 187-8502, Japan.

Authors' contributions

SatK conducted experiments, analyzed data, and wrote the manuscript. ShiK generated the *Iba1-GFP* transgenic mouse. SO designed experiments, and wrote the manuscript. All authors read and approved the final manuscript.

Competing interests

The authors declare that they have no competing interests.

Received: 27 April 2011 Accepted: 17 June 2011
Published: 17 June 2011

References

1. Streck EL, Comim CM, Barichello T, Quevedo J: **The septic brain.** *Neurochem Res* 2008, **33**:2171-2177.
2. Luheshi GN: **Cytokines and fever. Mechanisms and sites of action.** *Ann N Y Acad Sci* 1998, **856**:83-89.
3. Dinarello CA: **Cytokines as endogenous pyrogens.** *J Infect Dis* 1999, **179(Suppl 2)**:S294-304.
4. Cao C, Matsumura K, Yamagata K, Watanabe Y: **Involvement of cyclooxygenase-2 in LPS-induced fever and regulation of its mRNA by LPS in the rat brain.** *Am J Physiol* 1997, **272**:R1712-1725.
5. Matsumura K, Kaihatsu S, Imai H, Terao A, Shiraki T, Kobayashi S: **Cyclooxygenase in the vagal afferents: is it involved in the brain prostaglandin response evoked by lipopolysaccharide?** *Auton Neurosci* 2000, **85**:88-92.
6. Yamagata K, Matsumura K, Inoue W, Shiraki T, Suzuki K, Yasuda S, Sugiura H, Cao C, Watanabe Y, Kobayashi S: **Coexpression of microsomal-type prostaglandin E synthase with cyclooxygenase-2 in brain endothelial cells of rats during endotoxin-induced fever.** *J Neurosci* 2001, **21**:2669-2677.
7. Dantzer R, O'Connor JC, Freund GG, Johnson RW, Kelley KW: **From inflammation to sickness and depression: when the immune system subjugates the brain.** *Nat Rev Neurosci* 2008, **9**:46-56.
8. Shaw KN, Commins S, O'Mara SM: **Lipopolysaccharide causes deficits in spatial learning in the watermaze but not in BDNF expression in the rat dentate gyrus.** *Behav Brain Res* 2001, **124**:47-54.
9. Cunningham AJ, Murray CA, O'Neill LA, Lynch MA, O'Connor JJ: **Interleukin-1 beta (IL-1 beta) and tumour necrosis factor (TNF) inhibit long-term potentiation in the rat dentate gyrus *in vitro*.** *Neurosci Lett* 1996, **203**:17-20.
10. Commins S, O'Neill LA, O'Mara SM: **The effects of the bacterial endotoxin lipopolysaccharide on synaptic transmission and plasticity in the CA1-subiculum pathway *in vivo*.** *Neuroscience* 2001, **102**:273-280.
11. Giaume C, Kirchhoff F, Matute C, Reichenbach A, Verkhratsky A: **Glia: the fulcrum of brain diseases.** *Cell Death Differ* 2007, **14**:1324-1335.
12. Nakajima K, Kohsaka S: **Microglia: neuroprotective and neurotrophic cells in the central nervous system.** *Curr Drug Targets Cardiovasc Haematol Disord* 2004, **4**:65-84.
13. Hanisch UK, Kettenmann H: **Microglia: active sensor and versatile effector cells in the normal and pathologic brain.** *Nat Neurosci* 2007, **10**:1387-1394.
14. Ransohoff RM, Perry VH: **Microglial physiology: unique stimuli, specialized responses.** *Annu Rev Immunol* 2009, **27**:119-145.
15. Ohsawa K, Imai Y, Kanazawa H, Sasaki Y, Kohsaka S: **Involvement of Iba1 in membrane ruffling and phagocytosis of macrophages/microglia.** *J Cell Sci* 2000, **113(Pt 17)**:3073-3084.
16. Imai Y, Kohsaka S: **Intracellular signaling in M-CSF-induced microglia activation: role of Iba1.** *Glia* 2002, **40**:164-174.
17. Davalos D, Grutzendler J, Yang G, Kim JV, Zuo Y, Jung S, Littman DR, Dustin ML, Gan WB: **ATP mediates rapid microglial response to local brain injury *in vivo*.** *Nat Neurosci* 2005, **8**:752-758.
18. Nimmerjahn A, Kirchhoff F, Helmchen F: **Resting microglial cells are highly dynamic surveillants of brain parenchyma *in vivo*.** *Science* 2005, **308**:1314-1318.

19. Wake H, Moorhouse AJ, Jinno S, Kohsaka S, Nabekura J: **Resting microglia directly monitor the functional state of synapses *in vivo* and determine the fate of ischemic terminals.** *J Neurosci* 2009, **29**:3974-3980.
20. Okabe S, Kim HD, Miwa A, Kuriu T, Okado H: **Continual remodeling of postsynaptic density and its regulation by synaptic activity.** *Nat Neurosci* 1999, **2**:804-811.
21. Marrs GS, Green SH, Dailey ME: **Rapid formation and remodeling of postsynaptic densities in developing dendrites.** *Nat Neurosci* 2001, **4**:1006-1013.
22. Grutzendler J, Kasthuri N, Gan WB: **Long-term dendritic spine stability in the adult cortex.** *Nature* 2002, **420**:812-816.
23. Trachtenberg JT, Chen BE, Knott GW, Feng G, Sanes JR, Welker E, Svoboda K: **Long-term *in vivo* imaging of experience-dependent synaptic plasticity in adult cortex.** *Nature* 2002, **420**:788-794.
24. Zhang S, Boyd J, Delaney K, Murphy TH: **Rapid reversible changes in dendritic spine structure *in vivo* gated by the degree of ischemia.** *J Neurosci* 2005, **25**:5333-5338.
25. Zhang S, Murphy TH: **Imaging the impact of cortical microcirculation on synaptic structure and sensory-evoked hemodynamic responses *in vivo*.** *PLoS Biol* 2007, **5**:e119.
26. Tsai J, Grutzendler J, Duff K, Gan WB: **Fibrillar amyloid deposition leads to local synaptic abnormalities and breakage of neuronal branches.** *Nat Neurosci* 2004, **7**:1181-1183.
27. Meyer-Luehmann M, Spires-Jones TL, Prada C, Garcia-Alloza M, de Calignon A, Rozkalne A, Koenigsknecht-Talboo J, Holtzman DM, Bacskai BJ, Hyman BT: **Rapid appearance and local toxicity of amyloid-beta plaques in a mouse model of Alzheimer's disease.** *Nature* 2008, **451**:720-724.
28. Feng G, Mellor RH, Bernstein M, Keller-Peck C, Nguyen QT, Wallace M, Nerbonne JM, Lichtman JW, Sanes JR: **Imaging neuronal subsets in transgenic mice expressing multiple spectral variants of GFP.** *Neuron* 2000, **28**:41-51.
29. Hirasawa T, Ohsawa K, Imai Y, Ondo Y, Akazawa C, Uchino S, Kohsaka S: **Visualization of microglia in living tissues using Iba1-EGFP transgenic mice.** *J Neurosci Res* 2005, **81**:357-362.
30. Yuste R, Bonhoeffer T: **Genesis of dendritic spines: insights from ultrastructural and imaging studies.** *Nat Rev Neurosci* 2004, **5**:24-34.
31. Holtmaat A, Bonhoeffer T, Chow DK, Chuckowree J, De Paola V, Hofer SB, Hubener M, Keck T, Knott G, Lee WC, Mostany R, Mrsic-Flogel TD, Nedivi E, Portera-Cailliau C, Svoboda K, Trachtenberg JT, Wilbrecht L: **Long-term, high-resolution imaging in the mouse neocortex through a chronic cranial window.** *Nat Protoc* 2009, **4**:1128-1144.
32. Xu HT, Pan F, Yang G, Gan WB: **Choice of cranial window type for *in vivo* imaging affects dendritic spine turnover in the cortex.** *Nat Neurosci* 2007, **10**:549-551.
33. Zuo Y, Lin A, Chang P, Gan WB: **Development of long-term dendritic spine stability in diverse regions of cerebral cortex.** *Neuron* 2005, **46**:181-189.
34. Yang G, Pan F, Gan WB: **Stably maintained dendritic spines are associated with lifelong memories.** *Nature* 2009, **462**:920-924.
35. Yasumatsu N, Matsuzaki M, Miyazaki T, Noguchi J, Kasai H: **Principles of long-term dynamics of dendritic spines.** *J Neurosci* 2008, **28**:13592-13608.
36. Guo LH, Schluesener HJ: **Acute but not chronic stimulation of glial cells in rat spinal cord by systemic injection of lipopolysaccharide is associated with hyperalgesia.** *Acta Neuropathol* 2006, **112**:703-713.
37. Qin L, Wu X, Block ML, Liu Y, Breese GR, Hong JS, Knapp DJ, Crews FT: **Systemic LPS causes chronic neuroinflammation and progressive neurodegeneration.** *Glia* 2007, **55**:453-462.
38. Graeber MB, Streit WJ: **Microglia: biology and pathology.** *Acta Neuropathol* 2010, **119**:89-105.
39. Sparkman NL, Kohman RA, Garcia AK, Boehm GW: **Peripheral lipopolysaccharide administration impairs two-way active avoidance conditioning in C57BL/6J mice.** *Physiol Behav* 2005, **85**:278-288.
40. Zuo Y, Yang G, Kwon E, Gan WB: **Long-term sensory deprivation prevents dendritic spine loss in primary somatosensory cortex.** *Nature* 2005, **436**:261-265.
41. Holtmaat A, Wilbrecht L, Knott GW, Welker E, Svoboda K: **Experience-dependent and cell-type-specific spine growth in the neocortex.** *Nature* 2006, **441**:979-983.
42. Shaw KN, Commins S, O'Mara SM: **Cyclooxygenase inhibition attenuates endotoxin-induced spatial learning deficits, but not an endotoxin-induced blockade of long-term potentiation.** *Brain Res* 2005, **1038**:231-237.
43. Beattie EC, Stellwagen D, Morishita W, Bresnahan JC, Ha BK, Von Zastrow M, Beattie MS, Malenka RC: **Control of synaptic strength by glial TNFalpha.** *Science* 2002, **295**:2282-2285.
44. Ikegaya Y, Delcroix I, Iwakura Y, Matsuki N, Nishiyama N: **Interleukin-1beta abrogates long-term depression of hippocampal CA1 synaptic transmission.** *Synapse* 2003, **47**:54-57.
45. Centonze D, Muzio L, Rossi S, Cavasinni F, De Chiara V, Bergami A, Musella A, D'Amelio M, Cavallucci V, Martorana A, Bergamaschi A, Cencioni MT, Diamantini A, Butti E, Comi G, Bernardi G, Cecconi F, Battistini L, Furlan R, Martino G: **Inflammation triggers synaptic alteration and degeneration in experimental autoimmune encephalomyelitis.** *J Neurosci* 2009, **29**:3442-3452.
46. Okabe S, Miwa A, Okado H: **Spine formation and correlated assembly of presynaptic and postsynaptic molecules.** *J Neurosci* 2001, **21**:6105-6114.
47. Ullian EM, Sapperstein SK, Christopherson KS, Barres BA: **Control of synapse number by glia.** *Science* 2001, **291**:657-661.
48. Murai KK, Nguyen LN, Irie F, Yamaguchi Y, Pasquale EB: **Control of hippocampal dendritic spine morphology through ephrin-A3/EphA4 signaling.** *Nat Neurosci* 2003, **6**:153-160.
49. Nishida H, Okabe S: **Direct astrocytic contacts regulate local maturation of dendritic spines.** *J Neurosci* 2007, **27**:331-340.
50. Boulanger LM: **Immune proteins in brain development and synaptic plasticity.** *Neuron* 2009, **64**:93-109.
51. Lucin KM, Wyss-Coray T: **Immune activation in brain aging and neurodegeneration: too much or too little?** *Neuron* 2009, **64**:110-122.

doi:10.1186/1756-6606-4-27
Cite this article as: Kondo *et al.*: Long-term changes of spine dynamics and microglia after transient peripheral immune response triggered by LPS *in vivo*. *Molecular Brain* 2011 4:27.

Published OnlineFirst on October 5, 2011; DOI:10.1158/1078-0432.CCR-11-1712

Clinical Cancer Research

Predictive Biomarkers and Personalized Medicine

See commentary by Lauring and Park, p. 7808

Quantitative Detection of *EGFR* Mutations in Circulating Tumor DNA Derived from Lung Adenocarcinomas

Kazuya Taniguchi[1], Junji Uchida[2], Kazumi Nishino[2], Toru Kumagai[2], Takako Okuyama[2], Jiro Okami[3], Masahiko Higashiyama[3], Ken Kodama[3], Fumio Imamura[2], and Kikuya Kato[1]

Abstract

Purpose: Examination of somatic epidermal growth factor receptor (*EGFR*) mutations is now a diagnostic routine for treatment of cancer using EGFR tyrosine kinase inhibitors (EGFR-TKI). Circulating tumor DNA is a promising target for noninvasive diagnostics. We evaluated its utility by quantitatively detecting activating and resistant mutations, which were measured with BEAMing (beads, emulsion, amplification, and magnetics).

Experimental Design: Twenty-three patients with lung cancer with progressive disease after EGFR-TKI treatment and 21 patients who had never been treated with EGFR-TKIs were studied. Their primary tumors were confirmed to have activating mutations. In the plasma DNA of each patient, the activating mutation found in the corresponding primary tumor and the T790M resistance mutation were quantified by BEAMing.

Results: In 32 of 44 patients, activating mutations were detected in the plasma DNA [72.7%; 95% confidence interval (CI), 58.0%–83.6%]. The T790M mutation was detected in 10 of 23 patients in the first group (43.5%; 95% CI, 25.6%–53.4%). The ratio of T790M to activating mutations ranged from 13.3% to 94.0%. The peak of the distribution of the mutation allele fraction in the plasma DNA was in the 0.1% to 1% range.

Conclusions: The major advantage of BEAMing is its ability to calculate the fraction of T790M-positive alleles from the alleles with activating mutations. This feature enables the detection of increases and decreases in the number of T790M mutations in cancer cells, regardless of normal cell DNA contamination, which may be useful for monitoring disease progression. Circulating tumor DNA could potentially be used as an alternative method for *EGFR* mutation detection. *Clin Cancer Res; 17(24); 1–8. ©2011 AACR.*

Introduction

The strong effects of epidermal growth factor receptor (EGFR) tyrosine kinase inhibitors (EGFR-TKI; i.e., gefitinib and erlotinib) on non–small cell lung cancer (NSCLC) are correlated with activating somatic mutations in the epidermal growth factor receptor (*EGFR*; refs. 1–3). Patients subjected to these drugs are currently selected on the basis of the presence of these activating mutations. In addition, a mutation known as T790M has been identified as a cause of gefitinib resistance (4, 5). The T790M mutation appears in about half of the cases of acquired resistance to EGFR-TKIs. Detection of T790M may have prognostic value in the patients with acquired resistance to EGFR-TKIs, because the presence of T790M defines a clinical subset with a relatively favorable prognosis and more indolent progression (6).

Detecting *EGFR* mutations using tumor tissues obtained via a biopsy or surgical resection is now routinely used to diagnose NSCLC. Because a biopsy is an invasive procedure, it is desirable to replace it with a noninvasive procedure. In particular, noninvasive tests allow the frequent monitoring of disease progression in patients with the T790M mutation (7).

For some time, circulating nucleic acids in the plasma or serum have been considered to be candidates for noninvasive cancer diagnostics (8, 9). In particular, circulating tumor DNA (ctDNA) has been explored to detect somatic mutations derived from malignant tumors. For example, in 2 studies, somatic mutations in ctDNA were used to monitor disease status with the appearance of target mutations (10, 11). One major problem is that detecting rare mutant alleles is technically difficult. Diehl and colleagues used their proprietary technique called BEAMing (beads, emulsion, amplification and magnetics; ref. 12) to measure somatic mutations in ctDNA and monitor the tumor burden during the course of the disease. In BEAMing, PCR

Authors' Affiliations: [1]Research Institute, Departments of [2]Thoracic Oncology and [3]Thoracic Surgery, Osaka Medical Center for Cancer and Cardiovascular Diseases, Higashinari-ku, Osaka, Japan

Corresponding Author: Kikuya Kato, Research Institute, Osaka Medical Center for Cancer and Cardiovascular Diseases, 1-3-3 Nakamichi, Higashinari-ku, Osaka 537-8511, Japan. Phone: 81-6-6973-1209; Fax: 81-6-6973-1209; E-mail: katou-ki@mc.pref.osaka.jp

doi: 10.1158/1078-0432.CCR-11-1712

Published OnlineFirst on October 5, 2011; DOI:10.1158/1078-0432.CCR-11-1712

Translational Relevance

For therapies using EGFR-TKIs (e.g., gefitinib and erlotinib), it is essential to determine the epidermal growth factor receptor mutation status of lung cancer lesions. Although a biopsy of the primary lesion is indispensable, noninvasive diagnostics are desirable because they allow repeated testing. In particular, it is useful to follow the disease progression by monitoring the T790M status. In contrast to other techniques, beads, emulsion, amplification, and magnetics (BEAMing) can estimate the extent to which the activating mutation alleles have been converted into resistant alleles, regardless of normal DNA contamination. This information should be more suitable for monitoring the disease status. Because BEAMing also detects activating mutations with a moderate success rate, examining the ctDNA may support a diagnosis via a biopsy. It should be noted that BEAMing and next-generation sequencers are based on the same technological principle. With this study, we can predict how next generation sequencers will detect mutations in circulating tumor DNA.

products amplified from a single molecule are fixed to a single magnetic bead using emulsion PCR. The mutation site is labeled with a fluorescent probe or primer extension, and the mutated allele is quantitatively detected by counting the fluorescently labeled beads. Simply by increasing the number of beads that are analyzed, BEAMing can be more sensitive than other PCR-based techniques (13).

In this report, we used BEAMing to detect activating and resistant *EGFR* mutations in ctDNA derived from lung cancer. The results suggest that ctDNA may complement the biopsy of primary lesions as a source of *EGFR* mutation detection. Its major advantage over other techniques is its ability to calculate the fraction of T790M-positive alleles in cancer cells, regardless of normal cell DNA contamination. In particular, this approach would enable the monitoring of disease progression during EGFR-TKI therapy via the T790M mutation.

Materials and Methods

Patient characteristics

Patients with activating *EGFR* mutations in tumor tissues were selected following a biopsy examination between June 2010 and April 2011. We recruited 23 patients with progressive disease (PD) after EGFR-TKI treatment as group 1. PD is defined as the appearance of a new lesion or a 20% increase in tumor size. The duration between the detection of PD and blood sampling for BEAMing was variable. We recruited 21 patients who had never been treated with EGFR-TKIs as group 2. In all of the patients, activating EGFR mutations were found in biopsy samples using the PNA-LNA PCR clamp method (14).

Plasma samples and DNA extraction

DNA was purified from plasma obtained from 5 mL of heparin-treated blood using Agencourt Genfind version 2 (Beckman Coulter). The DNA concentration was determined by measuring the copy number of *LINE-1* (15). It should be noted that the calibration was done using intact human genomic DNA, whereas the plasma DNA was in fragments of approximately 200 bp or less. Thus, the deduced measurement may be biased to be too low.

BEAMing

BEAMing was done as described previously (16, 17), except for the use of locked nucleic acids (LNA) as the hybridization probes for single-base substitutions. Primer and probe sequences are shown in Table 1. In the initial PCR step, the target region (~100 bp) was amplified using gene-specific primers with tag sequences. Amplification was done in a 100-μL reaction mixture containing genomic DNA obtained from 400 μL of plasma, 600 pmol of primers and 2 units of KOD -Plus- DNA polymerase (Toyobo). The product was purified with a MinElute PCR Purification Kit (Qiagen).

To prepare the magnetic beads for BEAMing, a common oligonucleotide, the sequence of which was identical to the forward primer for emulsion PCR (Table 1), was synthesized using a dual biotin group at the 5′ end and a spacer 18 polyethylene glycol between the biotin group and the terminal thymidine (Integrated DNA Technologies). One nanomole of the common oligonucleotide was attached to 100 μg of MyOne streptavidin-coated magnetic beads (Dynal), as described previously (12). The beads were finally suspended in 100 μL of TK buffer (20 mmol/L Tris-HCl, pH 8.4, 50 mmol/L KCl). To prepare the emulsifier oil, 7% ABIL WE09 (Degussa), 20% mineral oil (Sigma-Aldrich) and 73% Tegosoft DEC (Degussa) were mixed by vortexing and allowed to settle for 30 minutes.

Emulsion PCR was done as follows. A 150-μL reaction mixture consisted of 15 pg of the first aforementioned PCR product, 15 μL of 10× KOD buffer, 75 pmol of the forward primer, 12 μmol of the reverse primer and 6 μL of the magnetic beads, which were prepared as described above. Next, 0.6 mL of the emulsifier oil and 5-mm Zirconia beads were added to the 150-μL reaction mixture. A water–oil emulsion was prepared in a 2-mL Eppendorf tube using a Mixer Mill MM 300 (Qiagen) at 15 Hz for 17 seconds. The reaction mixture was divided into 50-μL aliquots and amplified using the following thermal cycling protocol: 94°C for 2 minutes; 3 cycles of 98°C for 15 seconds, 64°C for 45 seconds, and 72°C for 75 seconds; 3 cycles of 98°C for 15 seconds, 61°C for 45 seconds, and 72°C for 75 seconds; 3 cycles of 98°C for 15 seconds, 58°C for 45 seconds, and 72°C for 75 seconds; and 50 cycles of 98°C for 15 seconds, 57°C for 45 seconds, and 72°C for 75 seconds.

After thermal cycling, the reaction mixture was centrifuged to separate the oil and water. After removing the supernatant, the emulsion was degraded with 400 μL of breaking buffer (5 mmol/L Tris-HCl, pH 7.5, 1% Triton X-100, 1% SDS, 100 mmol/L NaCl, 1 mmol/L EDTA) and by

Table 1. Primer list

	Name	Sequence	Modification	Target
Primers for exon amplification from plasma DNA				
exon19	Tag119del	TCCCGCGAAATTAATACGACAAGTTAAAATTCCCGTCGCTATC		
	Tag219del	GCTGGAGCTCTGCAGCTAGACCCCCACACAGCAAAG		
exon20	Tag1T790M	TCCCGCGAAATTAATACGACGCATCTGCCTCACCTCCAC		
	Tag2T790M	GCTGGAGCTCTGCAGCTAAGCAGGTACTGGGAGCCAAT		
exon21	Tag1L858R	TCCCGCGAAATTAATACGACAGCCAGGAACGTACTGGTGA		
	Tag2L858R	GCTGGAGCTCTGCAGCTATGCCTCCTTCTGCATGGTAT		
Primers for emulsion PCR				
	Tag1 (forward)	TCCCGCGAAATTAATACGAC		
	Tag2 (reverse)	GCTGGAGCTCTGCAGCTA		
Hybridization probes for detection of beads with successful amplification				
exon19	19del_BEAM_PE_b	AGCAAAGCAGAAACTCACATC	5′ biotin	
exon20	T790M_BEAM_PE_b	CGGACATAGTCCAGGAG	5′ biotin	
exon21	L858R_BEAM_PE_b	ATGCCTCCTTCTGCATGGTAT	5′ biotin	
Hybrizationprobe for BEAMing				
exon19	19del_35_49_647	GGAGATGTTTTGATAGCG	5′ Alexa647	exon 19 E746-A750del
	19del_36_50_647	CGGAGATGTCTTGATAGC	5′ Alexa647	exon 19 E746-A750del
	19del_40_57_647	TGGCTTTCGATTCCTTGA	5′ Alexa647	exon 19 L747-S752del.P753S
	19del_AATTCC_647	TGTTGCTTCTCTTGGAATT	5′ Alexa647	exon 19 E746-L747del.IP
	19del_36_55_T_647	GCTTTCGGAACCTTGATAG	5′ Alexa647	exon 19 L747-S752del. E746V
	19del_35_53_ACT_647	GGAGAAGTTTTGATAGCG	5′ Alexa647	exon 19 K745-E749del.A750K
	19del_39_56_CAG_647	TTTCGGCTGTTCCTTGAT	5′ Alexa647	exon 19 L747-T751del.S752Q
	19del_39_48_C_647	GAGATGTTGGTTCCTTGAT	5′ Alexa647	exon 19 L747-E749del.A750P
	19del_WT_488	TGTTGCTTCTCTTAATTCC	5′ Alexa488	exon 19 wild-type control
exon20	T790M_Mut_BNA_647	atgagctgcAtgatgag	5′ Alexa647	*T790M* mutation
	T790M_WT_BNA_488	tgagctgcGtgatgag	5′ Alexa488	Wild-type control for T790M
exon21	L858R_Mut_LNA_647	gtttggccCgcccaaaat	5′ Alexa647	*L858R* mutation
	L858R_WT_LNA_488	gtttggccAgcccaaaat	5′ Alexa488	Wild-type control for L858R
	T2582A_Mut_647	cacccagcTgtttggcc	5′ Alexa647	*T2582A* mutation
	T2582A_WT_488	cacccagcAgtttggcc	5′ Alexa488	Wild-type control for T2582A

Published OnlineFirst on October 5, 2011; DOI:10.1158/1078-0432.CCR-11-1712

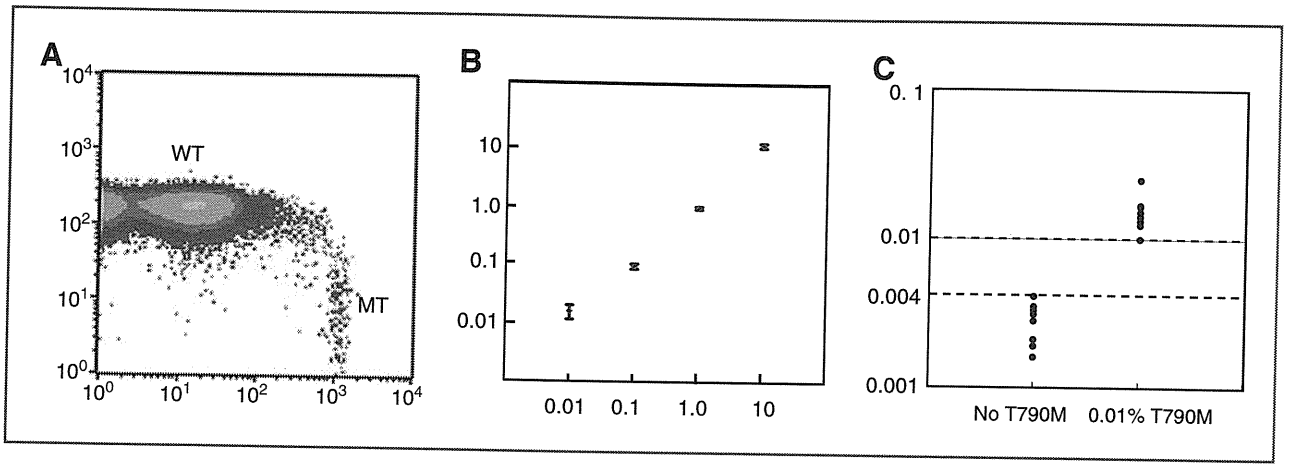

Figure 1. A, flow cytometric profile of BEAMing. The wild-type *EGFR* fragment was mixed with 0.1% of the T790M *EGFR* fragment, and BEAMing was done after PCR amplification. Horizontal axis, the fluorescence intensity of Alexa 647; vertical axis, the fluorescence intensity of Alexa 488. WT, signals from the wild-type *EGFR* fragment; MT, signals from the T789M fragment. B, linear correlation between the inoculated amount of the T790M *EGFR* fragment and the BEAMing measurement. Horizontal axis, the fraction of the T790M fragment inoculated into the wild-type fragment; vertical axis, the fraction of the T790M-positive allele measured using BEAMing. C, repeated measurements of the samples with 0.01% of the T790M fragment and those with no T790M fragment. The vertical axis indicates the fractions of the T790M-positive allele detected using BEAMing.

vortexing. After centrifugation and removal of the supernatant, the beads were washed once. Next, the DNA on the beads was denatured by 2 minutes of incubation at room temperature with 500 μL of 0.1 mol/L NaOH. After washing twice, the beads were suspended in 30 μL of distilled water.

The mutation loci were detected using allele-specific hybridization probes that consisted of locked nucleic acids and were fluorescence-labeled at their 5′ ends. Alexa 647 and Alexa 488 fluorescent dyes were used for the mutated and wild-type alleles, respectively. A hybridization probe complementary to common sequences in the mutated and wild-type alleles was manufactured via 5′ biotinylation. The hybridization reactions were carried out in a 100-μL reaction mixture consisting of 3 mol/L tetramethylammonium chloride, 50 mmol/L Tris-HCl (pH 7.5), 4 mmol/L EDTA, and 5 pmol each of the aforementioned hybridization probes. The reaction mixture was divided into 50 μL aliquots, incubated at 70°C for 10 seconds, then at 35 °C for 2 minutes after cooling down at a rate of 0.1°C/s, and additionally cooled down to room temperature using the GeneAmp PCR System 9700 Thermal Cycler (Applied Biosystems). After removing the supernatant, the beads were incubated at room temperature for 10 minutes in 20 μL of binding buffer (5 mmol/L Tris-HCl, pH 7.5, 1 mol/L NaCl, 1 mmol/L EDTA) containing 2 μg of streptavidin-conjugated phycoerythrin (PE; Invitrogen). After washing, the beads were suspended in 100 μL of TK buffer. Flow cytometric analysis was conducted with FACSCalibur (BD Bioscience) according to the manufacturer's protocol.

Results

Quantitation of the accuracy and sensitivity of BEAMing

We examined the measurement's accuracy and sensitivity using T790M as an example. We prepared normal *EGFR* gene fragments containing the mutated fragment at 10%, 1%, 0.1%, and 0.01%. These preparations were subjected to emulsion PCR. A typical example of a flow cytometric profile separating 1% T790M from the wild-type allele is shown in Fig. 1A. In BEAMing, the fractions of the mutated fragment are estimated by the ratio of the numbers of beads labeled with Alexa 647 (mutant) and those labeled with Alexa 488 (wild-type). There is a good linear correlation between the ratio deduced from the numbers of beads and the fraction of mutated fragments in the initial preparations (Fig. 1B). To determine the detection limit of BEAMing, samples without the T790M mutation and samples with 0.01% T790M mutations were analyzed repeatedly. The measurements of these 2 groups did not overlap (Fig. 1C). To confirm this result in a real experimental setting, we measured exon 19 deletion, L858R, and T790M mutations in the plasma DNA purified from 20 normal individuals. The mutation rates ranged from 0 to 0.0094 (average, 0.0021; 95% CI, 0.0012–0.0030), from 0.0009 to 0.0074 (average, 0.0025; 95% CI, 0.0019–0.0031) and from 0.0011 to 0.0097 (average, 0.0042; 95% CI 0.0030–0.0054), respectively. Thus, we set the detection limit of BEAMing as 1 in 10,000.

Activating and resistant *EGFR* mutations in plasma DNA

Plasma obtained from 44 patients was analyzed by BEAMing for the *T790M* mutation, and activating mutations were determined via a tumor biopsy. The results are shown in Table 2. In group 1, which consisted of patients who developed PD after EGFR-TKI treatment, the detection of activating and *T790M* mutations can be evaluated. In group 2, which consisted of patients who were never treated with EGFR-TKI, only those with activating mutations were evaluated. Most of the cases were in stage IV when their plasma DNA was obtained. In 32 of 44 patients, activating

Published OnlineFirst on October 5, 2011; DOI:10.1158/1078-0432.CCR-11-1712

Table 2. Allele frequency of activating and resistant *EGFR* mutations

Patient	Age, y	Sex	Histology	Stage	T790M, %	Activating mutation, %	T790M/activating mutation, %	Activating mutation type
A. Group 1 (patients with PD after EGFR-TKI treatment)								
1	56	M	adeno	4	0.029	0.058	50.8	L861Q
2	58	F	adeno	4	0.26	0.28	94.0	L858R
3	70	F	adeno	4	2.61	7.39	35.3	L858R
4	78	M	adeno	3A	0.08	0.13	65.0	L858R
5	65	M	Adeno + Sq	4	0.63	1.10	57.6	L858R
6	20	M	Adeno	4	0.14	1.03	13.3	exon 19 E746-A750del
7	41	F	adeno	4	4.28	10.3	41.6	exon 19 E746-A750del
8	59	F	adeno	4	9.54	42.7	22.3	exon 19 E746-A750del
9	53	M	adeno	4	0.16	0.19	83.6	exon 19 E746-A750del
10	49	F	adeno	4	ND	0.12	0.0	L861Q
11	75	F	adeno	4	ND	2.03	0.0	L858R
12	34	M	adeno	4	ND	0.33	0.0	L858R
13	64	M	adeno	4	ND	12.2	0.0	L858R
14	73	F	adeno	4	ND	0.046	0.0	L858R
15	66	F	adeno	4	ND	0.28	0.0	exon 19 L747-S752del.P753S
16	70	M	adeno	4	ND	11.5	0.0	exon 19 L747-S752del.P753S
17	44	F	adeno	4	ND	0.09	0.0	exon 19 L747-E749del.A750P
18	52	M	adeno	4	ND	0.74	0.0	exon 19 L747-E749del.A750P
19	74	F	adeno	4	ND	0.33	0.0	exon 19 E746-A750del
20	63	F	adeno	4	ND	ND	NA	L858R
21	65	F	adeno	4	0.10	ND	NA	exon 19 E746-A750del
22	51	F	adeno	4	ND	ND	NA	exon 19 E746-A750del
23	62	F	adeno	4	ND	ND	NA	exon 19 E746-A750del
B. Group 2 (patients not treated with EGFR-TKI)								
24	68	M	adeno	4	ND	0.17	0.0	L858R
25	45	F	adeno	4	ND	0.23	0.0	L858R
26	85	F	adeno	2B	ND	0.25	0.0	L858R
27	67	F	adeno	4	ND	0.079	0.0	L858R
28	58	F	adeno	4	ND	0.013	0.0	L858R
29	39	F	adeno	3B	ND	36.4	0.0	L858R
30	36	F	adeno	4	ND	0.11	0.0	exon 19 L747-S752del.E746V
31	56	M	adeno	4	ND	6.47	0.0	exon 19 L747-T751del.S752Q
32	55	F	adeno	3A	ND	6.24	0.0	exon 19 L747-E749del.A750P
33	65	F	adeno	3B	ND	11.8	0.0	exon 19 E746-A750del
34	76	F	adeno	4	ND	1.06	0.0	exon 19 E746-A750del
35	63	F	Sq	4	ND	0.73	0.0	exon 19 E746-A750del
36	63	M	adeno	4	ND	0.030	0.0	exon 19 E746-L747del.IP
37	72	F	adeno	4	ND	ND	NA	L858R
38	70	F	adeno	4	ND	ND	NA	L858R
39	63	M	adeno	4	ND	ND	NA	L858R
40	80	F	adeno	4	ND	ND	NA	L858R
41	70	F	adeno	4	ND	ND	NA	L858R
42	72	M	adeno	4	0.03	ND	NA	exon 19 L747-S752del.P753S
43	47	M	adeno	4	ND	ND	NA	exon 19 E746-A750del
44	54	F	adeno	4	ND	ND	NA	exon 19 E745-E749del.A750K

Abbreviations: NA, not applicable; ND, not detected.

mutations were detected in the plasma DNA (72.7%; 95% CI, 58.0–83.6%). The detection rate was higher in group 1 (group 1, 82.6%; group 2, 61.9%), but this difference was not statistically significant (the Fischer exact test, $P = 0.18$).

The detection rates of L858R/L861Q and exon 19 deletion were identical (72.7%). The T790M mutation was detected in 10 of 23 patients in group 1 (43.5%; 95% CI, 25.6%–53.4%). Because T790M accounted for about half of the

Published OnlineFirst on October 5, 2011; DOI:10.1158/1078-0432.CCR-11-1712

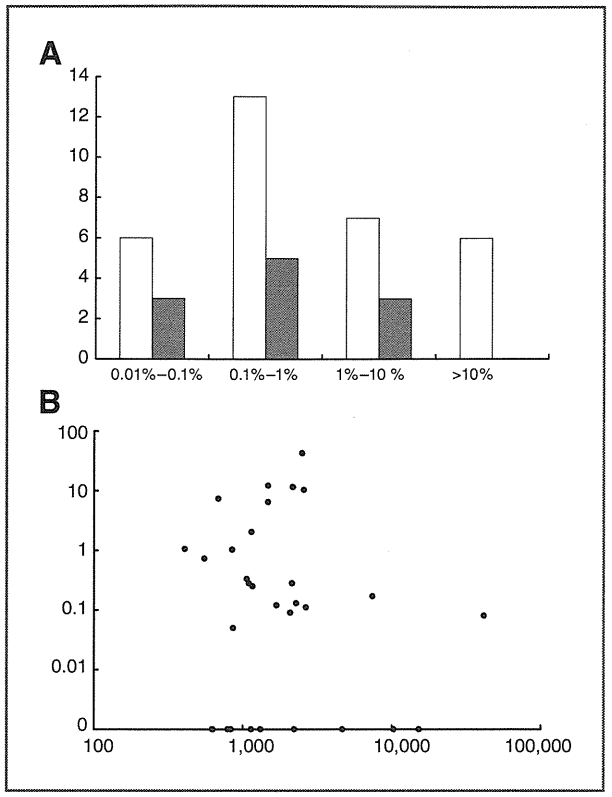

Figure 2. A, distribution of the fraction of *EGFR* molecules with activating (white columns) or resistant (gray columns) mutations in the plasma DNA. Horizontal axis, the percentage of activating EGFR mutations; vertical axis, the number of patients. B, relationship between the amount of recovered plasma DNA and the fraction of activating *EGFR* mutations. Horizontal axis, the amount of recovered plasma DNA (pg) corresponding to 400 μL of plasma; vertical axis, the percentage of activating *EGFR* mutations.

TKI-resistant cases, BEAMing was likely to detect T790M in most of the eligible cases. There were 2 cases of T790M mutations without an activating mutation (i.e., patients 21 and 42).

The fraction of ctDNA in plasma DNA can be estimated from the fraction of *EGFR* mutations [Table 2, activating mutations (%)]. On the basis of the histogram in Fig. 2A, the fraction of activating mutations varied widely across patients, and the peak of the distribution was in the 0.1% to 1% range. The fraction of the *T790M* mutation was distributed similarly but tended to shift toward lower percentages. We also investigated the relationship between the amount of recovered plasma DNA and the ctDNA deduced from the activating mutations, but we found no relationship between them (Fig. 2B). It should be noted that *EGFR* mutations were not detected in some samples with a high plasma DNA recovery.

We can deduce the number of tumor *EGFR* alleles that have been converted into resistant forms (i.e., T790M) by calculating the ratio of T790M to the number of activating mutation fractions. The ratios were within a range of 13.3% to 94.0% (Table 2), in contrast to a much wider range of tumor alleles in the plasma DNA.

Discussion

There have been a number of studies on the analysis of ctDNA to detect *EGFR* mutations in the serum or plasma DNA of NSCLC patients. These studies have mainly used techniques based on selective amplification (18, 19) or digestion (19) of specific alleles and/or high-throughput separation techniques [i.e., MALDI-TOF (20) or denaturing high performance liquid chromatography (DHPLC) (19, 21)]. The sensitivity is restricted by the specificity of the primers and enzymes in the former and by the signal-to-noise ratio in the latter. Because the sensitivity of BEAMing is only restricted by the mutations introduced during PCR (which is common to all techniques), it is theoretically more sensitive than other methods.

In addition to its high sensitivity, BEAMing allows the digital quantification of mutant alleles. The DNA in blood is derived from both tumor cells and normal cells, but we still do not know how the DNA in blood is generated. The major advantage of BEAMing is its ability to calculate the fraction of T790M-positive alleles from alleles with activating mutations. This feature enables the monitoring of the fractions of the T790M mutation in cancer cells, regardless of normal cell DNA contamination. This information should be more suitable for monitoring disease statuses. Some patients were reported to have cancer cells with T790M as a minor subpopulation before EGFR-TKI treatment (22, 23). With these cases, a qualitative assay to monitor T790M is inappropriate, and it is desirable to monitor amount of the T790M allele quantitatively. The fraction of the T790M allele would increase during the EGFR-TKI therapy and eventually reach a threshold to acquire resistance. Such threshold can be determined only with a quanititative assay. Partly due to difficulty of the biopsy of recurrent cases, clinical features of T790M-based resistance have not been fully understood, but are currently intensively studied. Such studies would find applications of the quantitative assay. For example, detecting the T790M mutation in blood samples would be useful for patient selection for treatment with new EGFR-TKIs for lung cancers that are resistant to gefitinib and erlotinib (24). One of such agents, PF00299804, is effective to a T790M-positive cell line. However, amplification of the T790M allele led to resistant to PF00299804 (25). If PF00299804 acts in patients in the same manner, quantitative monitoring of T790M allele would be useful for detection of resistance. In such patients, a biopsy of the tumor tissue is difficult and noninvasive diagnostics are highly beneficial.

The aim of this study is the initial demonstration of the technique, and has limitations as a clinical study. The patients were not enrolled in this study prospectively, and the timing of blood draws was not consistent such that the results are not directly applicable to distinct clinical situations. In addition, patients did not have serial tumor biopsies to document development of T790M in their cancer after exposure to EGFR-TKI. A well-designed prospective study enrolling more than 200 Japanese patients, a population with high incidence of activating mutation, now

Published OnlineFirst on October 5, 2011; DOI:10.1158/1078-0432.CCR-11-1712

being planned to validate present observations. It should be noted that specificity, that is, absence of pseudopositive, is most important for new noninvasive diagnostics. The validation study should also be focused on this point as well.

As suggested by a recent review (26), the most problematic aspect of ctDNA analysis is the difficulty in purifying DNA from the blood. As described above, the amount of plasma DNA varies by 2 orders of magnitude. The cause of this variation (i.e., whether it is due to true variation or the low reproducibility of the purification procedure) is unknown. However, it should be noted that unsuccessful mutation detection was not necessarily frequent in the cases with low DNA recovery and that unsuccessful mutation detection was still found among those with abundant DNA recovery. Some cases of low DNA recovery contained the minimum number of *EGFR* copies for detection. In such cases, whole-genome amplification is beneficial for sound PCR and may enhance the detection rate, as seen in a previous study (19).

This study focused on advanced lung cancer (mainly stage IV lung cancer). If ctDNA analysis is effective for early lung cancer, then it may be applicable to early cancer detection. Because ctDNA is also easily detected in the early stages of colorectal cancer (27), it is worthwhile to test ctDNA analysis for early lung cancer.

BEAMing uses the template preparation step of massively parallel sequencers (so-called next-generation sequencers; ref. 28). Therefore, we can predict the outcome when massively parallel sequencers are applied to this problem. The recent development of a new sequencer (29) has addressed the shortcomings of currently available sequencers (i.e., a long runtime for a single assay and high operating costs), and would be suitable for diagnostic purposes. The cost of sequencing is still rapidly decreasing, and will be eventually negligible in the total cost of the assay. In contrast to BEAMing, which analyzes only a single base and requires information about mutations in primary tumors, the massively parallel sequencers obtain information from more than a hundred bases and could replace BEAMing. A recent study pointed out the need for repeated sequencing to overcome the high error rates of the sequencers that are currently used to detect rare mutations (30). However, in the case of *EGFR* mutations, because the mutation sites are already known, rare mutations may be detected with a statistical method without the repeated sequencing. Our study forecasts the outcome of ctDNA analysis using massively parallel sequencers, suggesting that ctDNA analysis could determine the *EGFR* mutation status of more than 70% of advanced lung cancer cases. In addition, there might be cases in which *EGFR* mutations could be detected only with ctDNA analysis, not with a conventional biopsy. Given the noninvasive nature of the ctDNA analysis, it is a worthwhile field for future investigation.

Disclosure of Potential Conflicts of Interest

No potential conflicts of interest were disclosed.

Grant Support

This work was partly supported by KAKENHI 20890299 and 23790636.
The costs of publication of this article were defrayed in part by the payment of page charges. This article must therefore be hereby marked *advertisement* in accordance with 18 U.S.C. Section 1734 solely to indicate this fact.

Received July 4, 2011; revised September 20, 2011; accepted September 23, 2011; published OnlineFirst October 5, 2011.

References

1. Lynch TJ, Bell DW, Sordella R, Gurubhagavatula S, Okimoto RA, Brannigan BW, et al. Activating mutations in the epidermal growth factor receptor underlying responsiveness of non-small-cell lung cancer to gefitinib. N Engl J Med 2004;350:2129–39.
2. Paez JG, Janne PA, Lee JC, Tracy S, Greulich H, Gabriel S, et al. EGFR mutations in lung cancer: correlation with clinical response to gefitinib therapy. Science 2004;304:1497–500.
3. Rosell R, Moran T, Queralt C, Porta R, Cardenal F, Camps C, et al. Screening for epidermal growth factor receptor mutations in lung cancer. N Engl J Med 2009;361:958–67.
4. Kobayashi S, Boggon TJ, Dayaram T, Janne PA, Kocher O, Meyerson M, et al. EGFR mutation and resistance of non-small-cell lung cancer to gefitinib. N Engl J Med 2005;352:786–92.
5. Pao W, Miller VA, Politi KA, Riely GJ, Somwar R, Zakowski MF, et al. Acquired resistance of lung adenocarcinomas to gefitinib or erlotinib is associated with a second mutation in the EGFR kinase domain. PLoS Med 2005;2:e73.
6. Oxnard GR, Arcila ME, Sima CS, Riely GJ, Chmielecki J, Kris MG, et al. Acquired resistance to EGFR tyrosine kinase inhibitors in EGFR-mutant lung cancer: distinct natural history of patients with tumors harboring the T790M mutation. Clin Cancer Res 2011;17:1616–22.
7. Kosaka T, Yatabe Y, Endoh H, Yoshida K, Hida T, Tsuboi M, et al. Analysis of epidermal growth factor receptor gene mutation in patients with non-small cell lung cancer and acquired resistance to gefitinib. Clin Cancer Res 2006;12:5764–9.
8. Goebel G, Zitt M, Zitt M, Muller HM. Circulating nucleic acids in plasma or serum (CNAPS) as prognostic and predictive markers in patients with solid neoplasias. Dis Markers 2005;21:105–20.
9. Vlassov VV, Laktionov PP, Rykova EY. Circulating nucleic acids as a potential source for cancer biomarkers. Curr Mol Med 2010;10:142–65.
10. Diehl F, Schmidt K, Choti MA, Romans K, Goodman S, Li M, et al. Circulating mutant DNA to assess tumor dynamics. Nat Med 2008;14:985–90.
11. Shinozaki M, O'Day SJ, Kitago M, Amersi F, Kuo C, Kim J, et al. Utility of circulating B-RAF DNA mutation in serum for monitoring melanoma patients receiving biochemotherapy. Clin Cancer Res 2007;13:2068–74.
12. Dressman D, Yan H, Traverso G, Kinzler KW, Vogelstein B. Transforming single DNA molecules into fluorescent magnetic particles for detection and enumeration of genetic variations. Proc Natl Acad Sci U S A 2003;100:8817–22.
13. Pao W, Ladanyi M. Epidermal growth factor receptor mutation testing in lung cancer: searching for the ideal method. Clin Cancer Res 2007;13:4954–5.
14. Nagai Y, Miyazawa H, Huqun, Tanaka T, Udagawa K, Kato M, et al. Genetic heterogeneity of the epidermal growth factor receptor in non-small cell lung cancer cell lines revealed by a rapid and sensitive detection system, the peptide nucleic acid-locked nucleic acid PCR clamp. Cancer Res 2005;65:7276–82.
15. Rago C, Huso DL, Diehl F, Karim B, Liu G, Papadopoulos N, et al. Serial assessment of human tumor burdens in mice by the analysis of circulating DNA. Cancer Res 2007;67:9364–70.

Published OnlineFirst on October 5, 2011; DOI:10.1158/1078-0432.CCR-11-1712

16. Diehl F, Schmidt K, Durkee KH, Moore KJ, Goodman SN, Shuber AP, et al. Analysis of mutations in DNA isolated from plasma and stool of colorectal cancer patients. Gastroenterology 2008;135:489–98.
17. Li M, Chen WD, Papadopoulos N, Goodman SN, Bjerregaard NC, Laurberg S, et al. Sensitive digital quantification of DNA methylation in clinical samples. Nat Biotechnol 2009;27:858–63.
18. Kimura H, Kasahara K, Kawaishi M, Kunitoh H, Tamura T, Holloway B, et al. Detection of epidermal growth factor receptor mutations in serum as a predictor of the response to gefitinib in patients with non-small-cell lung cancer. Clin Cancer Res 2006;12:3915–21.
19. Kuang Y, Rogers A, Yeap BY, Wang L, Makrigiorgos M, Vetrand K, et al. Noninvasive detection of EGFR T790M in gefitinib or erlotinib resistant non-small cell lung cancer. Clin Cancer Res 2009;15:2630–6.
20. Brevet M, Johnson ML, Azzoli CG, Ladanyi M. Detection of EGFR mutations in plasma DNA from lung cancer patients by mass spectrometry genotyping is predictive of tumor EGFR status and response to EGFR inhibitors. Lung Cancer 2011;73:96–102.
21. Bai H, Mao L, Wang HS, Zhao J, Yang L, An TT, et al. Epidermal growth factor receptor mutations in plasma DNA samples predict tumor response in Chinese patients with stages IIIB to IV non-small-cell lung cancer. J Clin Oncol 2009;27:2653–9.
22. Inukai M, Toyooka S, Ito S, Asano H, Ichihara S, Soh J, et al. Presence of epidermal growth factor receptor gene T790M mutation as a minor clone in non-small cell lung cancer. Cancer Res 2006;66:7854–8.
23. Soh J, Toyooka S, Ichihara S, Suehisa H, Kobayashi N, Ito S, et al. EGFR mutation status in pleural fluid predicts tumor responsiveness and resistance to gefitinib. Lung Cancer 2007;56:445–8.
24. Giaccone G, Wang Y. Strategies for overcoming resistance to EGFR family tyrosine kinase inhibitors. Cancer Treat Rev 2011;37:456–64.
25. Ercan D, Zejnullahu K, Yonesaka K, Xiao Y, Capelletti M, Rogers A, et al. Amplification of EGFR T790M causes resistance to an irreversible EGFR inhibitor. Oncogene 2010;29:2346–56.
26. Schwarzenbach H, Hoon DS, Pantel K. Cell-free nucleic acids as biomarkers in cancer patients. Nat Rev Cancer 2011;11:426–37.
27. Diehl F, Li M, Dressman D, He Y, Shen D, Szabo S, et al. Detection and quantification of mutations in the plasma of patients with colorectal tumors. Proc Natl Acad Sci U S A 2005;102:16368–73.
28. Margulies M, Egholm M, Altman WE, Attiya S, Bader JS, Bemben LA, et al. Genome sequencing in microfabricated high-density picolitre reactors. Nature 2005;437:376–80.
29. Rothberg JM, Hinz W, Rearick TM, Schultz J, Mileski W, Davey M, et al. An integrated semiconductor device enabling non-optical genome sequencing. Nature 2011;475:348–52.
30. Kinde I, Wu J, Papadopoulos N, Kinzler KW, Vogelstein B. Detection and quantification of rare mutations with massively parallel sequencing. Proc Natl Acad Sci U S A 2011;108:9530–5.

Clin Exp Metastasis (2011) 28:427–435
DOI 10.1007/s10585-011-9381-0

RESEARCH PAPER

Dynamics of cancer cell subpopulations in primary and metastatic colorectal tumors

Teodora Evgenieva Goranova · Masayuki Ohue · Yutaro Shimoharu · Kikuya Kato

Received: 23 December 2010 / Accepted: 17 February 2011 / Published online: 5 March 2011

Abstract Intratumor heterogeneity—heterogeneity of cancer cells within a single tumor—is considered one of the most problematic factors of treatment. Genetic heterogeneity, such as in somatic mutations and chromosome aberrations, is a common characteristic of human solid tumors and is probably the basis of biological heterogeneity. Using mutations in *APC*, *TP53* and *KRAS* as markers to identify distinct colorectal cancer subpopulations, we analyzed a total of 42 primary colorectal cancer tissues and six paired liver metastases with multipoint microsampling, which enabled analysis of mutation patterns and allelic imbalances with a resolution of 0.01 mm^2 (about 200 cells). There was usually more than one subpopulation in each primary tumor. Only two of 15 (13.3%) cases with three gene mutations and eight of 27 (29.6%) cases with two gene mutations had a single subpopulation. Cells with mutations in all of the examined genes usually constituted the major population. Multipoint microsampling of six primary and metastatic tumor pairs revealed that the majority of discrepancies in mutation patterns found with the bulk tissue analysis were due to loss of subpopulations in the metastatic tissues. In addition, multipoint microsampling uncovered substantial changes in subpopulations that were not detected with bulk tissue analysis. Specifically, the proportion of *KRAS* mutation-negative subpopulations increased in the metastatic tumors of four cases. Because *KRAS* mutation status is linked to cetuximab/panitumumab efficacy, subpopulation dynamics could lead to differences in response to cetuximab/panitumumab in primary versus metastatic tumors.

Keywords Intratumor heterogeneity · Molecular target drug · Colorectal cancer · Somatic mutation

Abbreviations
CSC Cancer stem cell
SAP Shrimp alkaline phosphatase

Electronic supplementary material The online version of this article (doi:10.1007/s10585-011-9381-0) contains supplementary material, which is available to authorized users.

T. E. Goranova · Y. Shimoharu · K. Kato (✉)
Research Institute, Osaka Medical Center for Cancer and Cardiovascular Diseases, 1-3-3 Nakamichi, Higashinari-ku, Osaka 537-8511, Japan
e-mail: katou-ki@mc.pref.osaka.jp

M. Ohue
Department of Surgery, Osaka Medical Center for Cancer and Cardiovascular Diseases, 1-3-3 Nakamichi, Higashinari-ku, Osaka 537-8511, Japan

Present Address:
T. E. Goranova
Molecular Medicine Center, 2 Zdrave Street, 1431 Sofia, Bulgaria

Introduction

Intratumor heterogeneity, which is the heterogeneity of cancer cells within a single tumor, is considered one of the most problematic factors of treatment. During anti-cancer therapy, the initial regression of the tumor eventually leads to the outgrowth of drug-resistant cells. Resistant cells likely exist in a heterogeneous primary cancer cell population rather than evolve from it. A recently emerging topic related to heterogeneity is the cancer stem cell (CSC) hypothesis [1], which assumes that only a fraction of cancer cells have the

ability to initiate tumor formation. In addition, the CSC hypothesis claims that currently available drugs are not effective because they target the total cancer cell population.

In addition to the heterogeneity of biological features presented by CSC, genetic heterogeneity, such as in somatic mutations and chromosome aberrations, is a common characteristic of human solid tumors and is probably the basis of biological heterogeneity. A number of studies have described genetic heterogeneity [2–11]. Although these studies have demonstrated that cancer cell subpopulations with different mutation patterns are present in most solid tumors, there were several technical limitations. In particular, these studies did not use laser microdissection, which is now a standard technique, and they had a relatively high threshold of detection, which may have hampered the detection of rare clones.

Genetic heterogeneity within primary tumors is a single aspect of tumor heterogeneity. Although tumors develop at one site, some cancer cells leave the primary tumor and develop metastases at distant sites. Because metastases account for the majority of cancer-related deaths, understanding the underlying mechanism of their development is extremely important. Analysis of genetic heterogeneity, such as in somatic mutations, may help clarify the issue. Although intratumor heterogeneity has been intensely studied, the question of heterogeneity within metastases remains unexplored [12].

Colorectal cancer is one of the most common and well-studied cancer types. Because somatic mutations in the *APC*, *KRAS* and *TP53* genes have been established as "drivers" for colorectal carcinogenesis [13], we chose these genes as markers to identify cancer cell subpopulations. We analyzed a total of 42 primary colorectal cancer tissues and 6 paired metastatic tissues with multipoint microsampling [11, 14], which is our proprietary technical approach for analyzing intratumor genetic heterogeneity. Multipoint microsampling enables analysis of mutation patterns and allelic imbalance with a resolution of 0.01 mm^2 (about 200 cells). We examined the prevalence of intratumor genetic heterogeneity in primary tumors and the dynamics of cancer cell subpopulations in primary and metastatic tumors.

Materials and methods

Samples

In a previous study, a total of 86 bulk primary colorectal cancer tissues from our tumor tissue bank were examined for mutations in the *APC*, *KRAS* and *TP53* genes. DNA was extracted from frozen bulk tumor tissues using the QIAamp DNA Micro Kit (Qiagen, Hilden, Germany), and the coding regions of *APC*, *KRAS* and *TP53* were examined for mutations using High-Resolution Melting on a LightScanner (Idaho Technology, Salt Lake City, UT, USA). Samples with aberrant melting curves were analyzed using direct sequencing with the BigDye Terminator Cycle Sequencing Kit (ver. 3.1, Applied Biosystems, Carlsbad, CA, USA) on an ABI PRISM 3730 (Applied Biosystems). Cases with a single mutation, in which cells with no mutation were the only heterogeneous subpopulation, were excluded because such a subpopulation was difficult to distinguish from normal epithelial cells. Forty-two primary colorectal cancer tissues were included in the present study: 15 tumor tissues with mutations in all three genes (i.e., *APC*, *KRAS* and *TP53* genes) and 27 tumors with only two mutated genes. The details of the mutations in these tumors are listed in Table S1. In addition, 6 liver metastatic tissues from the cases with mutations in all three genes were included in the study. The present study was approved by the Ethical Committee of the Osaka Medical Center for Cancer and Cardiovascular Diseases, and informed consent was obtained from all patients.

Multipoint microsampling

For the analysis of intratumor heterogeneity, 40-μm-thick sections from frozen cancer tissues were prepared on a Leica CM1900 cryostat (Leica Microsystems, Wetzlar, Germany) and stained with Mayer's hematoxylin (Wako, Osaka, Japan). Forty to fifty small areas (100 × 100 μm) containing only tumor cells were microdissected from each sample. Microdissection was performed using the Leica AS LMD system (Leica Microsystems). The sampling was randomized, but we avoided repeated sampling from the same region. Genomic DNA was extracted using the prepGEM Kit (ZyGEM, Hamilton, New Zealand), according to the manufacturer's protocol, and a 20-μl DNA mixture was prepared from each sample.

PCR amplification and SNaPshot assay

For each case, the DNA fragments that were found to contain mutations in bulk tissue analysis were simultaneously amplified using multiplex PCR on a GeneAmp PCR System 9700 (Applied Biosystems). The PCR was performed in a 10-μl reaction volume including 5 μl DNA (approximately 250 pg), 1× PCR buffer (Applied Biosystems), 2 mM $MgCl_2$, 200 μM of each dNTP, 0.2 μM of each primer (Table S2) and 1 U AmpliTaqGold polymerase (Applied Biosystems). The cycling conditions consisted of an initial denaturation step at 94°C for 5 min, 40 cycles of denaturing at 94°C for 30 s, annealing at 54–56°C for 30 s, extension at 72°C for 40 s and a final synthesis at 72°C for 5 min.

The mutation status was quantitatively determined using the SNaPshot assay. Each primer was designed to bind to a complementary template immediately adjacent to the

mutation site. The reaction was carried out in the presence of fluorescently labeled ddNTPs, and DNA polymerase was used to extend the primer by one nucleotide (adding a single ddNTP to its 3′ end). The following fluorescent dyes were used for the dideoxynucleotides: A, dR6G; C, dTAMRA; G, dR110; and T, dROX.

The PCR fragments were prepared for primer extension by incubating a mixture containing 7.5 μl PCR product, 0.5 U shrimp alkaline phosphatase (SAP) (TaKaRa, Otsu, Japan) and 1 U exonuclease I (TaKaRa) in a final volume of 10 μl at 37°C for 40 min, which was followed by inactivation of the enzymes at 80°C for 20 min. Primer extension was carried out in a 5-μl reaction, which contained 2 μl treated PCR product, 2.5 μl ABI Prism SNaPshot Multiplex Ready Reaction Mix (Applied Biosystems) and 0.5 μl extension primer mix (0.2 μM of each primer). The primer sequences are shown in Table S2. The cycling conditions, which were carried out according to the manufacturer's protocol, included 25 cycles of denaturation at 96°C for 10 s, annealing at 50°C for 5 s and extension at 60°C for 30 s. To remove the unincorporated ddNTPs, 5 μl of the SNaPshot products was incubated for 40 min at 37°C with 0.5 U SAP (TaKaRa) in a final volume of 6 μl, and the enzyme was inactivated as described above. A 1-μl aliquot of the treated SNaPshot reaction was denatured in 9 μl distilled water in the presence of GeneScan 120 LIZ Size Standard (Applied Biosystems) for 5 min at 95°C and analyzed on an ABI PRISM 3100 Genetic Analyzer (Applied Biosystems). Fragment analysis was performed with Gene Mapper Software v4.0 (Applied Biosystems).

Data analysis

The mutation status of each area was determined by calculating the mutant allele ratio (ΔM) for each gene using the following equation: $\Delta M = M/(M + N)$, where M is the mutant allele peak height and N is the normal peak height. The reproducibility of amplification and the SNaPshot assay was confirmed in our previous experiments [14]. In most cases of mutant allele loss, the corresponding peak height (M) was zero. However, there were several areas with residual peaks where we set the threshold for ΔM at 0.05.

Results

Intratumor heterogeneity of primary colorectal cancers

In a previous study, we established a method called multipoint microsampling to characterize genetic heterogeneity in colorectal cancer using laser microdissection [11, 14]. This method has two characteristics: (1) a sample size small enough to keep contamination from other cell populations to a minimum, but large enough to ensure unbiased amplification, and (2) a high enough sample number (~50) to obtain reproducible results from minor

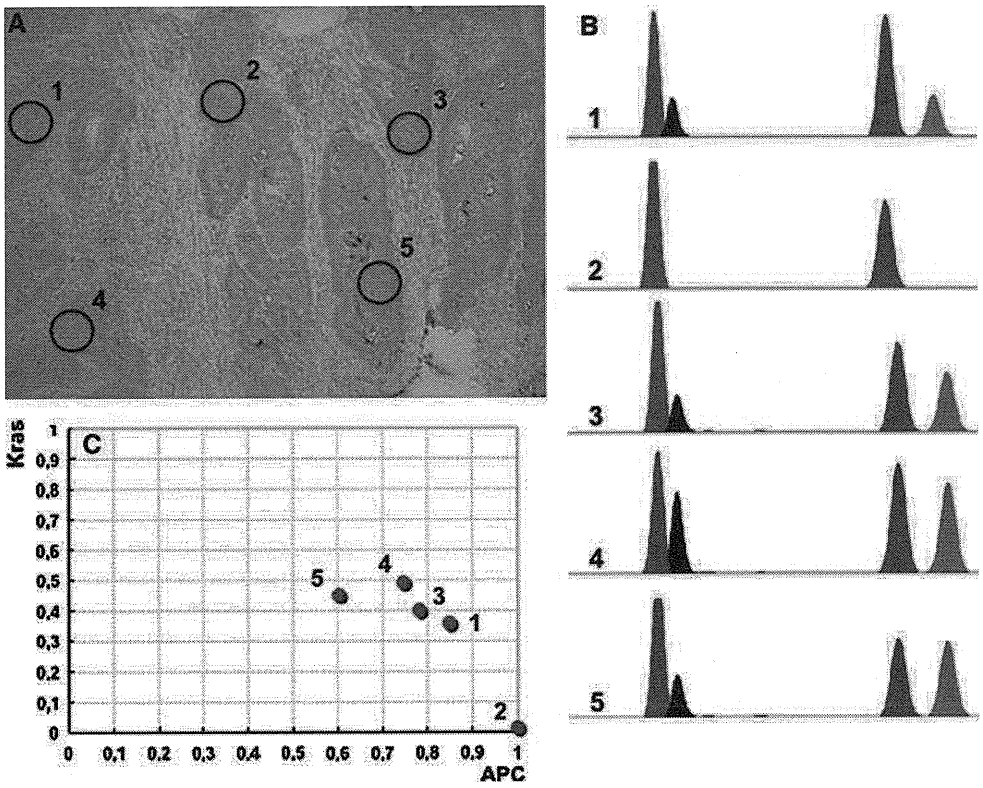

Fig. 1 An example of intratumor heterogeneity. **a** A microscopic view of a colorectal cancer tissue section with *black circles* indicating the microdissected areas (1–5). **b** Electropherograms of the SNaPshot assay. The first two peaks represent the mutation status of *APC* (C>G), and the second two peaks represent the mutation status of *KRAS* (G>A). The *blue* peak is a fragment amplified with ddG, the *black* peak is a fragment amplified with ddC and the *green* peak is a fragment amplified with ddA. **c** Graphic representation of the SNaPshot results. The mutant allele ratio (ΔM) of *APC* is plotted on the *x*-axis, and the ΔM of *KRAS* is plotted on the *y*-axis

Table 1 Summary of the genotypes in the 42 primary tumors

Case	Clinical stage	Samples/tumor	Clone	Genotype			Areas	%	AIH[b]-APC	AIH[b]-KRAS	AIH[b]-TP53
				APC mut[a]	*KRAS* mut[a]	*TP53* mut[a]					
1	IV	42	A	−	−	+	3	7,1	+	+	+
			B	+	−	+	1	2,4			
			C	+	+	+	38	90,5			
3	II	48	A	−	+	+	2	4,2	+	+	+
			B	+	+	+	46	95,8			
11	III	41	A	+	−	−	7	17,1	+	+	−
			B	+	+	−	4	9,8			
			C	+	+	+	30	73,2			
19	III	45	A	−	+	+	2	4,4	+	+	+
			B	+	+	+	43	95,6			
24	II	49	A	+	−	+	2	4,1	+	+	+
			B	+	+	+	47	95,9			
33	IV	48	A	+	−	−	21	43,8	−	+	+
			B	+	+	−	9	18,8			
			C	+	+	+	18	37,5			
41	III	40	A	−	−	+	7	17,5	+	+	+
			B	−	+	+	1	2,5			
			C	+	+	+	32	80			
49[c]	IV	40	A	+/+	+	+	40	100	+	+	−
51	IV	42	A	−	−	+	1	2,4	+	+	+
			B	+	−	+	2	4,8			
			C	+	+	+	39	92,9			
65	IV	49	A	+	−	−	2	4,1	+	+	+
			B	+	−	+	2	4,1			
			C	+	+	+	45	91,8			
74	I	41	A	+	+	+	41	100	+	−	+
81	IV	42	A	+	+	−	4	9,5	+	+	+
			B	+	+	+	38	90,5			
82	IV	48	A	+	−	+	1	2,1	+	+	+
			B	−	−	+	3	6,3			
			C	−	+	+	41	85,4			
			D	+	+	+	1	2,1			
83	IV	45	A	+	+	−	4	8,9	+	+	+
			B	+	+	+	41	91,1			
85	IV	44	A	+	−	+	1	2,3	+	+	+
			B	−	+	−	2	4,5			
			C	−	−	+	1	2,3			
			D	−	+	+	35	79,5			
			E	+	+	+	5	11,4			
4	III	44	A	+	+	−	44	100	+	+	ND
6	II	40	A	+	+	−	40	100	−	−	ND
12	III	49	A	+	−	−	13	26,5	+	+	ND
			B	+	+	−	36	73,5			
13	II	45	A	−	+	−	1	2,2	+	+	ND
			B	+	+	−	44	97,8			

Table 1 continued

Case	Clinical stage	Samples/tumor	Clone	Genotype			Areas	%	AIH[b]-APC	AIH[b]-KRAS	AIH[b]-TP53
				APC mut[a]	*KRAS* mut[a]	*TP53* mut[a]					
18	III	46	A	+	−	−	1	2,2	+	+	ND
			B	+	+	−	45	97,8			
21	II	50	A	−	+	−	2	4	+	−	ND
			B	+	+	−	48	96			
57	III	50	A	+	+	−	50	100	−	−	ND
8[c]	III	50	A	+/+	−	−	3	6	+	ND	+
			B	−	−	+	9	18			
			C	+	−	+	8	16			
			D	+/+	−	+	30	60			
9	IV	50	A	+	−	+	50	100	+	ND	−
17	III	47	A	+	−	−	1	2,1	+	ND	+
			B	−	−	+	3	6,4			
			C	+	−	+	43	91,5			
20	II	42	A	+	−	−	4	9,5	+	ND	+
			B	−	−	+	3	7,1			
			C	+	−	+	35	83,3			
28	II	50	A	+	−	+	50	100	−	ND	+
36	I	50	A	+	−	+	50	100	+	ND	+
39	III	50	A	−	−	+	38	76	−	ND	+
			B	+	−	+	12	24			
43[c]	I	50	A	+	−	−	2	4	+	ND	+
			B	+	−	+	2	4			
			C	+/+	−	+	46	92			
46[c]	II	50	A	+	−	−	5	10	+	ND	+
			B	+	−	+/+	45	90			
48	III	41	A	−	−	+	2	4,9	+	ND	−
			B	+	−	+	39	95,1			
63[c]	II	50	A	+/+	−	−	1	2	+	ND	+
			B	+/+	−	+	49	98			
66	I	50	A	+	−	+	50	100	+	ND	+
67	III	49	A	−	−	+	18	36,7	+	ND	+
			B	+	−	+	31	63,3			
70	III	44	A	+	−	−	2	4,5	+	ND	+
			B	+	−	+	42	95,5			
75	III	40	A	+	−	−	5	12,5	+	ND	+
			B	+	−	+	35	87,5			
76	II	40	A	+	−	−	2	5	+	ND	+
			B	−	−	+	7	17,5			
			C	+	−	+	31	77,5			
10	II	49	A	−	−	+	5	10,2	ND	+	−
			B	−	+	+	44	89,8			
26	II	42	A	−	+	−	4	9,5	ND	+	+
			B	−	−	+	9	21,4			
			C	−	+	+	29	69			
47	III	50	A	−	+	+	50	100	ND	−	+

Table 1 continued

Case	Clinical stage	Samples/tumor	Clone	Genotype			Areas	%	AIH[b]-APC	AIH[b]-KRAS	AIH[b]-TP53
				APC mut[a]	*KRAS* mut[a]	*TP53* mut[a]					
64	I	46	A	–	+	–	23	50	ND	+	+
			B	–	+	+	23	50			

[a] *mut* mutations given in Table S1 for each tumor case

[b] *AIH* heterogeneity in allelic imbalance

[c] Cases with two mutations in one gene (case 8, 43, 46, 49, 63). "+/+" means two mutations, "+" one mutation, "–" no mutation in the gene. For case 8 single mutation in APC is c.3139 G>T; for case 43-c.904 C>T

populations. To detect mutations, we used the SNaPshot assay, which is a quantitative primer extension assay that yields ratios of mutated and normal alleles.

All 42 samples were subjected to multipoint microsampling. Figure 1 shows a microscopic image of a tumor tissue section from case 12 (Fig. 1a), an electropherogram of the SNaPshot assay (Fig. 1b) and a graphical presentation of the mutant allele ratios (ΔM) of *APC* and *KRAS* (Fig. 1c). Although all five regions in Fig. 1a contained cells with mutations in *APC*, not all of the regions carried mutations in *KRAS*; there was only one peak (ddG) for the *KRAS* allele in region 2 (Fig. 1b, c).

The mutation statuses of all samples taken from primary tumor tissues are summarized in Table 1. Representative results of areas from primary colorectal cancer tissues plotted in three dimensions were created using the ΔM values of *APC*, *KRAS* and *TP53*, and 2-D plots were made for the samples with two mutated genes. These results are shown in Fig. S1.

There was usually more than one subpopulation in each primary tumor. Indeed, only two of 15 (13.3%) cases with three gene mutations and eight of 27 (29.6%) cases with two gene mutations exhibited a single subpopulation. In most heterogeneous tumors, cells with all mutations constituted the major population (Table 1).

Because the SNaPshot assay measures relative levels of both alleles, we also revealed heterogeneity of allelic imbalance. Because the standard deviation of the SNaPshot assay was 0.08 [14], cases where the data ranges were over 0.32 ($\pm 2\sigma$) were considered heterogeneous. For example, case 10 showed heterogeneity in the allele ratio of *KRAS* (ΔM = 0.0–0.53), but not of *TP53* (ΔM = 0.94–1.0), whereas case 6 did not show heterogeneity for either of the two genes (ΔM = 0.46–0.61 for *KRAS* and 0.85–1.0 for *APC*) (Fig. S1). The status of the heterogeneity of allelic imbalance is shown in Table 1. The heterogeneity was probably due to a mixture of two or more cell subpopulations with different allelic ratios.

Comparison of intratumor genetic heterogeneity between primary and metastatic tumors

Among the 15 primary tumors with the three gene mutations, six cases had corresponding hepatic metastatic tumors. The details of mutations revealed by bulk tissue analysis are shown in Table 2. Except for two cases (82 and 85), metastatic tissues carried the same mutations as the corresponding primary tumors. We compared the intratumor heterogeneity of the three gene mutations between primary and metastatic tumors for each case. Table 3 summarizes the mutation status of subpopulations in the tissue pairs. The percentages of each subpopulation in a primary tumor and its paired metastasis are graphically presented for all six cases in Fig. 2.

Table 2 Mutations found by bulk tissue analysis of six pairs of primary and metastatic tumors

Case	Sample	*APC* mutation	*KRAS* mutation	*TP53* mutation
1	T	c.4348 C>T R1450[a]	c.34 G>T G12C	c.818 G>A R273H
	M	c.4348 C>T R1450[a]	c.34 G>T G12C	c.818 G>A R273H
51	T	c.2626 C>T R876[a]	c.35 G>T G12V	c.818 G>A R273H
	M	c.2626 C>T R876[a]	c.35 G>T G12V	c.818 G>A R273H
81	T	c.1690C>T R564[a]	c.183 A>T Q61H	c.524 G>A R175H
	M	c.1690C>T R564[a]	c.183 A>T Q61H	c.524 G>A R175H
82	T	c.2626 C>T R876[a]	c.34 G>A G12S	c.755_63 del 9 bp
	M	–	c.34 G>A G12S	c.755_63 del 9 bp
83	T	c.4147 insA	c.38 G>A G13D	c.682 ins 8 bp
	M	c.4147 insA	c.38 G>A G13D	c.682 ins 8 bp
85	T	c.2626 C>T R876[a]	c.35 G>T G12V	c.733 G>A G245S
	M	–	c.35 G>T G12V	c.733 G>A G245S

[a] Stop codon

Table 3 Cell populations found in primary tumors and metastases of the patients

Case	Clone	Genotype			Examined samples/ tumor	Areas in primary tumor[b]	%	Examined samples/ metastasis	Areas in metastasis[b]	%
		APC mut[a]	KRAS mut[a]	TP53 mut[a]						
1	A	–	–	c.818 G>A R273H	42	3	7.1	50	0	0
	B	c.4348 C>T R1450[c]	–	c.818 G>A R273H		1	2.4		36	72.0
	C	c.4348 C>T R1450[c]	c.34 G>T G12C	c.818 G>A R273H		38	90.5		14	28.0
51	A	–	–	c.818 G>A R273H	42	1	2.4	50	0	0
	B	c.2626 C>T R876[c]	–	c.818 G>A R273H		2	4.8		0	0
	C	c.2626 C>T R876[c]	c.35 G>T G12V	c.818 G>A R273H		39	92.9		50	100.0
81	A	c.1690C>T R564[c]	c.183 A>T Q61H	–	42	4	9.5	50	7	14.0
	B	c.1690C>T R564[c]	c.183 A>T Q61H	c.524 G>A R175H		38	90.5		43	86.0
82	A	c.2626 C>T R876[c]	–	c.755_63 del 9 bp	48	1	2.1	49	0	0
	B	–	–	c.755_63 del 9 bp		3	6.3		25	51.0
	C	–	c.34 G>A G12S	c.755_63 del 9 bp		41	85.4		24	49.0
	D	c.2626 C>T R876[c]	c.34 G>A G12S	c.755_63 del 9 bp		3	6.3		0	0
83	A	c.4147 insA	c.38 G>A G13D	–	45	4	8.9	50	0	0
	B	c.4147 insA	c.38 G>A G13D	c.682 ins 8 bp		41	91.1		50	100.0
85	A	c.2626 C>T R876[c]	–	c.733 G>A G245S	44	1	2.3	50	0	0
	B	–	c.35 G>T G12V	–		2	4.5		0	0
	C	–	–	c.733 G>A G245S		1	2.3		9	18.0
	D	–	c.35 G>T G12V	c.733 G>A G245S		35	79.5		41	82.0
	E	c.2626 C>T R876[c]	c.35 G>T G12V	c.733 G>A G245S		5	11.4		0	0

[a] *mut* mutation

[b] Number of samples with a specific genotype

[c] Stop codon

In cases 82 and 85, there were discrepancies of mutation patterns; both cases lacked *APC* mutations in metastatic tumors (Table 2). Indeed, multipoint microsampling revealed that metastatic tumors lacked subpopulations with an *APC* mutation in both cases (i.e., subpopulations A and D in case 82 and subpopulations A and E in case 85) (Table 3 and Fig. 2d and f).

In cases 51 and 83, the major subpopulation of the primary tumor occupied all areas of the metastatic tumor (Fig. 2b and e, respectively). This result suggests that at least most cancer cells in the liver metastases were derived from the major subpopulations of the primary tumors in these two cases. In other cases, there was more than one subpopulation within the metastatic tumor tissue. In all cases, there were no de novo mutations, which suggests that cells from subpopulations in the primary tumors moved to the liver. In cases 1, 82 and 85, the proportions of *KRAS* mutation-negative subpopulations increased (Fig. 2a, d and f, respectively). Because both the primary and metastatic tumors in case 1 were mostly composed of a single major subpopulation, we performed array-CGH to exclude the possibility that the *KRAS* mutant allele would be lost by LOH after metastasizing. Notably, there was no LOH in the KRAS region (data not shown), which suggests that the mutation-negative subpopulation of the metastatic tumor was derived from the minor mutation-negative subpopulation of the primary tumor.

Discussion

Multipoint microsampling offers much higher resolution than techniques used in similar studies in the literature [2–11]. Consequently, we found intratumor heterogeneity in 87% of primary tumors with mutations in three genes (i.e., *APC*, *KRAS* and *TP53*) and in 70% of tumors with mutations in two of the three genes. We then compared mutation statuses between primary and metastatic tumors. The multipoint microsampling approach revealed that discrepancies of mutation patterns found by bulk tissue analysis were due to loss of subpopulations in the metastatic tissues. In addition, multipoint microsampling uncovered substantial changes in subpopulations that were not detected by bulk tissue analysis, such as the increase of *KRAS* mutation-negative cells in metastatic tumors.

A recent study of exome sequencing in pancreatic cancer reported a similar finding. Indeed, clonal populations that give rise to distant metastases were represented in one of the subpopulations taken from several parts of the

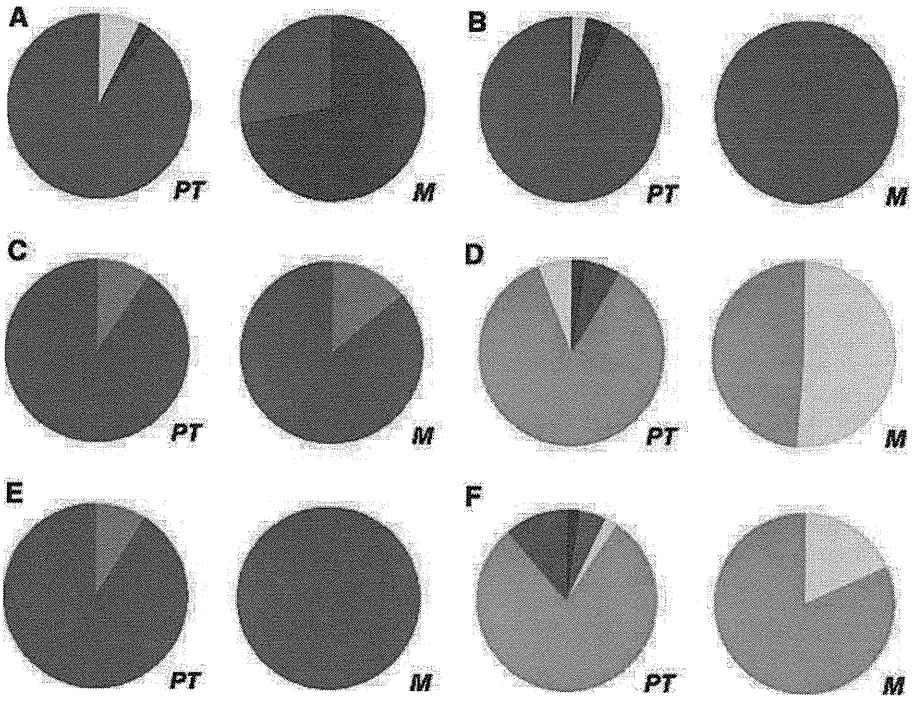

Fig. 2 Genetic heterogeneity in six pairs of primary and metastatic tumor tissues. The percentages of areas with a particular mutation status in the primary tumor (PT) and its paired metastasis (M) are graphically presented for each case. The mutation patterns are: $APC^{N}KRAS^{N}TP53^{M}$, *yellow*; $APC^{N}KRAS^{M}TP53^{N}$, *light purple*; $APC^{M}KRAS^{N}TP53^{M}$, *dark blue*; $APC^{N}KRAS^{M}TP53^{M}$, *green*; $APC^{M}KRAS^{M}TP53^{N}$, *light blue*; and $APC^{M}KRAS^{M}TP53^{M}$, *red* (M, mutated gene; N, no mutation). **a** Case 1, **b** case 51, **c** case 81, **d** case 82, **e** case 83, and **f** case 85

primary tumors [15]. This study by Campbell et al. identified far more mutations than our study. In addition, the Campbell et al. study identified the original parental non-metastatic clones from which metastatic clones evolved. In the present study, we used multipoint microsampling, which has a markedly greater spatial resolution because the exome sequencing study was based on DNA prepared from more than 100 million cells. We found that the metastatic tumors included more than one subpopulation of the primary tumor in four cases (Fig. 2). In liver metastases, colorectal cancer cells move to the liver via the portal vein, which differs from ordinary distant metastases where cells move through the systemic circulation. The simultaneous migration of more than one subpopulation might be specific to liver metastases of colorectal cancer because of this anatomical characteristic.

Clinical trials with cetuximab or panitumumab revealed that patients with wild-type *KRAS* responded to therapy (up to 50%), whereas those with tumors exhibiting *KRAS* mutations had a low response rate (0–6%) [16–21]. Although the *KRAS* mutation status is predictive of cetuximab/panitumumab efficacy, there are cases in which the response did not match the prediction. Based on a hypothesis that the heterogeneity of *KRAS* mutations between primary and metastatic tumors may be responsible for this discrepancy, Italiano et al. analyzed 95 pairs of primary and metastatic tumors. Italiano et al. found that *KRAS* was mutated in primary tumors in six cases, but wild-type *KRAS* was found in metastatic tumors. In addition, eight cases showed that *KRAS* was mutated in metastatic tumors, but wild-type *KRAS* was found in primary tumors [22]. Moreover, Baldus et al. analyzed 20 pairs of a primary tumor and a distant metastasis, and found heterogeneity of the *KRAS* mutation status in two cases [23]. Heterogeneity between primary and lymph node metastases was more frequent (31% of cases) than that between primary and metastatic tumors. Both studies indicated that the discrepancy of the *KRAS* mutation status between a primary tumor and its distant metastasis was likely to be too rare to account for the discordance between the *KRAS* mutation status and cetuximab/panitumumab efficacy. The results from these two studies, however, were obtained with analysis of bulk tissues or macrodissection. The present study demonstrated that there were changes in proportions of subpopulations that could not be detected by bulk tissue analysis. Thus, the possibility remains that heterogeneity of the *KRAS* mutation status could be the cause of altered cetuximab/panitumumab efficacy. Our preliminary study on intratumor heterogeneity of *EGFR* mutations in lung cancer suggested that tumors that have cancer cells with wild-type *EGFR* exhibited an inferior response to gefitinib [11]. Because molecularly targeted drugs are becoming the mainstream of adjuvant therapy, intratumor heterogeneity of target genes might be an important factor requiring further intensive analysis.

Acknowledgments The authors thank Dr Kazuya Taniguchi for technical advice. This work was partly supported by the Knowledge Cluster Initiative (the Keihanna Science City area) of the Ministry of Education, Culture, Sports, Science, and Technology of Japan.

References

1. Visvader JE, Lindeman GJ (2008) Cancer stem cells in solid tumours: accumulating evidence and unresolved questions. Nat Rev Cancer 8(10):755–768
2. Baisse B, Bouzourene H, Saraga EP et al (2001) Intratumor genetic heterogeneity in advanced human colorectal adenocarcinoma. Int J Cancer 93(3):346–352
3. Barnetson R, Jass J, Tse R et al (2000) Mutations associated with microsatellite unstable colorectal carcinomas exhibit widespread intratumoral heterogeneity. Genes Chromosomes Cancer 29(2): 130–136
4. Giaretti W, Rapallo A, Sciutto A et al (2000) Intratumor heterogeneity of k-ras and p53 mutations among human colorectal adenomas containing early cancer. Anal Cell Pathol 21(2):49–57
5. Gonzalez-Garcia I, Sole RV, Costa J (2002) Metapopulation dynamics and spatial heterogeneity in cancer. Proc Natl Acad Sci USA 99(20):13085–13089
6. Konishi N, Hiasa Y, Matsuda H et al (1995) Intratumor cellular heterogeneity and alterations in ras oncogene and p53 tumor suppressor gene in human prostate carcinoma. Am J Pathol 147 (4):1112–1122
7. Losi L, Baisse B, Bouzourene H et al (2005) Evolution of intratumoral genetic heterogeneity during colorectal cancer progression. Carcinogenesis 26(5):916–922
8. Lyng H, Beigi M, Svendsrud DH et al (2004) Intratumor chromosomal heterogeneity in advanced carcinomas of the uterine cervix. Int J Cancer 111(3):358–366
9. Samowitz WS, Slattery ML (1999) Regional reproducibility of microsatellite instability in sporadic colorectal cancer. Genes Chromosomes Cancer 26(2):106–114
10. Takeshima Y, Amatya VJ, Daimaru Y et al (2001) Heterogeneous genetic alterations in ovarian mucinous tumors: application and usefulness of laser capture microdissection. Hum Pathol 32(11): 1203–1208
11. Taniguchi K, Okami J, Kodama K et al (2008) Intratumor heterogeneity of epidermal growth factor receptor mutations in lung cancer and its correlation to the response to gefitinib. Cancer Sci 99(5):929–935
12. Marusyk A, Polyak K (2010) Tumor heterogeneity: causes and consequences. Biochim Biophys Acta 1805(1):105–117
13. Fearon ER, Vogelstein B (1990) A genetic model for colorectal tumorigenesis. Cell 61(5):759–767
14. Goranova TE, Ohue M, Kato K (2009) Putative precursor cancer cells in human colorectal cancer tissue. Int J Clin Exp Pathol 2(2):154–162
15. Campbell PJ, Yachida S, Mudie LJ et al (2010) The patterns and dynamics of genomic instability in metastatic pancreatic cancer. Nature 467(7319):1109–1113
16. De Roock W, Piessevaux H, De Schutter J et al (2008) KRAS wild-type state predicts survival and is associated to early radiological response in metastatic colorectal cancer treated with cetuximab. Ann Oncol 19(3):508–515
17. Di Fiore F, Blanchard F, Charbonnier F et al (2007) Clinical relevance of KRAS mutation detection in metastatic colorectal cancer treated by Cetuximab plus chemotherapy. Br J Cancer 96(8):1166–1169
18. Hecht JR, Patnaik A, Berlin J et al (2007) Panitumumab monotherapy in patients with previously treated metastatic colorectal cancer. Cancer 110(5):980–988
19. Khambata-Ford S, Garrett CR, Meropol NJ et al (2007) Expression of epiregulin and amphiregulin and K-ras mutation status predict disease control in metastatic colorectal cancer patients treated with cetuximab. J Clin Oncol 25(22):3230–3237
20. Lievre A, Bachet JB, Boige V et al (2008) KRAS mutations as an independent prognostic factor in patients with advanced colorectal cancer treated with cetuximab. J Clin Oncol 26(3): 374–379
21. Lievre A, Bachet JB, Le Corre D et al (2006) KRAS mutation status is predictive of response to cetuximab therapy in colorectal cancer. Cancer Res 66(8):3992–3995
22. Italiano A, Hostein I, Soubeyran I et al (2010) KRAS and BRAF mutational status in primary colorectal tumors and related metastatic sites: biological and clinical implications. Ann Surg Oncol 17(5):1429–1434
23. Baldus SE, Schaefer KL, Engers R et al (2010) Prevalence and heterogeneity of KRAS, BRAF, and PIK3CA mutations in primary colorectal adenocarcinomas and their corresponding metastases. Clin Cancer Res 16(3):790–799

ALCOHOLISM: CLINICAL AND EXPERIMENTAL RESEARCH

Vol. 35, No. 2
February 2011

Increased Serum Levels of Pigment Epithelium-Derived Factor by Excessive Alcohol Consumption—Detection and Identification by a Three-Step Serum Proteome Analysis

Kazuyuki Sogawa, Yoshio Kodera, Mamoru Satoh, Yusuke Kawashima, Hiroshi Umemura, Katsuya Maruyama, Hirotaka Takizawa, Osamu Yokosuka, and Fumio Nomura

Background: The search for biological markers of alcohol abuse is of continual interest in experimental and clinical alcohol research. We previously used gel-free proteome analysis methods such as the ProteinChip® system and the ClinProt™ system to search for new serum markers for alcoholism and found several novel marker candidates. As serum contains thousands of proteins and peptides that are present in a large dynamic concentration, depletion of the abundant proteins and further fractionation of the remainder is necessary to get into the deep proteome. We recently described a simple and highly reproducible three-step method for identifying potential disease-marker candidates among the low-abundance serum proteins.

Methods: Two serum samples—one on admission and one after 8 weeks of abstinence—were obtained from 8 patients with alcohol dependency. The samples were subjected to a three-step serum proteome analysis. The steps were the following: first, immunodepletion of the 6 most abundant proteins; second, fractionation using reverse-phase high-performance liquid chromatography; and third, separation using one-dimensional sodium dodecyl sulfate polyacrylamide gel electrophoresis (SDS–PAGE). Differences revealed by protein staining were further confirmed by Western blotting and by enzyme-linked immunosorbent assays (ELISA).

Results: Three-step serum proteome analysis revealed that the serum levels of 5 proteins, alpha2-HS glycoprotein, apolipoprotein A-I, glutathione peroxidase 3, heparin cofactor II, and pigment epithelial-derived factor (PEDF), were significantly greater on admission than after 8 weeks of abstinence. We focused on PEDF because alterations in its levels in alcoholic subjects are not well known. Western blotting and ELISA confirmed the upregulation of PEDF. Serum PEDF levels were significantly greater in moderate to heavy habitual drinkers (14.2 ± 7.7 μg/ml) than in healthy subjects without a drinking history (5.5 ± 3.0 μg/ml) ($p < 0.001$). The serum PEDF levels in subjects with nonalcoholic chronic liver diseases were comparable to the PEDF levels in healthy subjects.

Conclusion: Three-step serum proteome analysis reveals that excessive alcohol drinking increases the PEDF level.

Key Words: Alcoholism, Pigment Epithelial-Derived Factor, Proteomics, Serum.

EXCESSIVE ALCOHOL CONSUMPTION causes alcoholism and alcoholic liver diseases and aggravates many common medical problems such as hypertension, diabetes mellitus, and gout. Although the primary strategy for detecting heavy drinking relies on self-reporting, heavy drinkers tend to underestimate their alcohol consumption. This leads to an underdiagnosis of hazardous alcohol use and related disorders (Alling et al., 2005). Therefore, the search for biological markers of alcohol abuse is of continual interest in experimental and clinical alcohol research (Hannuksela et al., 2007; Niemela, 2007; Nomura et al., 2007).

We previously used the ProteinChip® system to search for new serum markers of alcoholism and found several novel marker candidates (Nomura et al., 2004). Of these markers, a 5.9-kDa peptide (which is a fragment of the fibrinogen alpha chain) with an *m/z* of 5890 was useful in detecting gamma-glutamyltransferase (GGT) nonresponders in male subjects seeking a medical checkup (Sogawa et al., 2007). More recently, we used the ClinProt™ system (Bruker Daltonics, Bremen, Germany; consisting of a combination of beads processing and matrix-assisted laser desorption/ionization

From the Clinical Proteomics Research Center (KS, YK, MS, YK, FN), Chiba University Hospital, Chiba, Japan; Department of Physics (YK), School of Science, Kitasato University, Kanagawa, Japan; Department of Molecular Diagnosis (HU, FN), Graduate School of Medicine, Chiba University, Chiba, Japan; National Hospital Organization Kurihama Alcoholism Center (KM), Kanagawa, Japan; Kashiwado Clinic in Port-Square (HT), Kashiwado Memorial Foundation, Chiba, Japan; and Division of Gastroenterology (OY), Chiba University Hospital, Chiba, Japan.

Received for publication April 26, 2010; accepted July 18, 2010.

Reprint requests: Fumio Nomura, MD, PhD, Department of Molecular Diagnosis, Graduate School of Medicine, Chiba University, 1-8-1 Inohana, Chuo-ku, Chiba City, Chiba 260-8670, Japan; Fax: +81-43-226-2324; E-mail: fnomura@faculty.chiba-u.jp

DOI: 10.1111/j.1530-0277.2010.01336.x